Academic Journal of Science and Technology
ISSN: 2771-3032 | Vol. 13, No. 1, 2024

DC Arc Plasma Numerical Simulation Calculation Review

Shuangliang Li, Jing Tao

School of Sichuan University of Science and Engineering, Zigong 643000, China

Abstract: This study established a three-dimensional numerical model based on the Fluent software, listing the commonly used boundary conditions, physical models, and basic assumptions in the process of DC arc plasma numerical simulation. By combining multiple literature analyses, the influence of working gas flow rate, working current magnitude, degree of gas swirl, and non-swirling gas on the internal physical fields of the DC arc plasma torch was investigated. The research results indicate that the temperature, current density, plasma flow velocity, and pressure inside the plasma torch all increase with the increase of the working gas flow rate and working current. Under the same operating conditions, an increase in the degree of gas swirl leads to a decrease in the temperature and current density inside the plasma torch. This study provides theoretical support for the design, optimization, and control of plasma torches, which is helpful in improving the thermal efficiency and application effects of plasma torches.

Keywords: DC Arc Plasma; Turbulence Models; Energy Conservation; Current Density; Joule Heating.

1. Introduction

Currently, in the field of DC arc plasma research, many scholars have conducted two-dimensional modeling with axisymmetric simplifications. However, the motion and heat transfer of the arc are three-dimensional phenomena. Therefore, two-dimensional research has its limitations in predicting and analyzing the arc. As a result, a large number of researchers have embarked on detailed analyses of the impact of the arc current, arc voltage, temperature field in the arc column region, heat flux on the fixed electrodes, and jet characteristics on practical applications such as spraying and cutting.

The team led by Wang Zhen studied the internal physical fields of the DC arc plasma torch through numerical simulation methods, focusing on the distribution forms of temperature and velocity fields. Through numerical calculations, it was found that the temperature at the exit of the plasma torch jet could reach 13,000 K, and the maximum flow velocity could reach 2,400 m/s. The study also revealed the relationship between the temperature distribution of high-temperature plasma and the current density distribution, as well as the influence of the anode structure on the jet velocity [1].

The team led by Wang Pingyang addressed the issues of numerical simulation and diagnostic analysis of the DC arc plasma torch by establishing a numerically coupled model of flow, heat transfer, and electromagnetism. They conducted three-dimensional numerical simulations using Fluent software. By designing a thermal enthalpy probe experimental system, the team measured the temperature and velocity parameters of the plasma torch jet and found that the numerical simulation results were in good agreement with the experimental measurements, verifying the accuracy of the model. In addition, they also studied the influence of different working gas flow rates on the temperature and velocity of the plasma torch, discovering a positive linear relationship between the highest temperature, maximum speed, and airflow rate. However, an excessive gas flow rate was found to reduce the average temperature of the plasma torch [2].

The team led by K. Bobzin, in their study of the multi-arc plasma spraying process, investigated the impact of a fixed nozzle extension on the characteristics of the plasma jet. To gain a deeper understanding of this phenomenon, the team used ANSYS CFX software to establish a numerical model and conducted relevant research. The study results showed that the extended design of the nozzle could significantly increase the temperature of the plasma. This finding suggests that even under lower processing parameter conditions, the nozzle extension could effectively achieve particle melting, thereby improving the total energy efficiency of the plasma spraying process. This research provides a theoretical basis for optimizing the design of plasma spraying nozzles and helps to enhance the efficiency and effectiveness of the spraying process [3].

The team led by Sebastian Manzke is dedicated to exploring the potential of plasma jets as an assist gas in laser melting cutting processes and conducted a comparative study with traditional nitrogen jet streams. The research first employed numerical simulation methods to analyze the fundamental characteristics of non-transferred plasma jets. Based on the simulation results, the team designed a DC non-transferred arc plasma torch and carried out actual cutting experiments [4].

The research group led by Zelong Zhang conducted in-depth research on a multi-cathode arc plasma source with a 20-mm anode channel. In the experiments, the team successfully obtained arc plasma images and arc voltage spectra under different discharge current conditions. The study found that at a current value of 30A, the arcs produced by each cathode remained in an independent state; when the current was increased to 50A, the cathode arcs coupled in the center of the arc chamber. The increase in current led to stabilization of the arc's voltage and spatial distribution. At the same time, the research team established a three-dimensional steady-state non-local thermal equilibrium model to calculate the temperature distribution, current density, and Lorentz force field of the multi-cathode plasma torch. The numerical simulation showed good consistency with the experimental data in terms of voltage. The numerical analysis indicated that with the increase in current, both the distribution of Lorentz forces and the current density showed an upward trend. The increase in current intensified the interaction between the arc plasmas. Additionally, compared to traditional arc torches, the multi-cathode plasma had a lower flow rate. The research findings contribute to understanding the generation mechanism of arc plasma in multi-cathode torches [5].

The research team led by Xudan Wang first conducted a detailed analysis of the plasma discharge phenomenon and fluid dynamics model. Subsequently, they used the drift-diffusion approximation to construct a set of control equations, which included the continuity equations for the heavy particle species, the calculation of the electric field distribution, and the volume forces. By integrating the plasma chemical kinetics model, they established a comprehensive model of plasma discharge. Following this, the team explored the interaction mechanism and discharge characteristics of radiofrequency plasma with the discharge process. In the final stage of the research, they performed numerical simulations on the magnetized radiofrequency plasma discharge process. The simulation results revealed that with the increase in discharge power, the electron density in the plasma showed an increasing trend [6].

The team led by Han Xiao established a model that coupled electricity and heat transfer with fluid dynamics through numerical simulation and experimental research to analyze the thermal efficiency of the DC arc plasma torch. By comparing the results, they verified the effectiveness of the model, providing theoretical support for the prediction of thermal efficiency and operational control of the plasma torch [7].

The team led by R. Abiyazhini conducted a comparative study of the characteristics of CO_2 and Ar plasma arcs and their application effects in material processing. By establishing a two-dimensional axisymmetric model, they simulated the behavior of both plasma arcs under conditions with and without anode evaporation, and investigated the influence of arc current and anode material. The study found that CO_2 plasma arcs have higher temperatures and anode heat fluxes compared to Ar plasma arcs, and the arc current has a more significant impact on their temperature and anode heat flux. The heating efficiency of CO_2 plasma arcs is higher, but it decreases with increasing current. Despite the advantages of CO_2 plasma arcs in terms of material processing efficiency, the issue of anode material oxidation that it may cause requires further investigation. In summary, CO_2 plasma arcs have broad application potential in material processing fields such as nano powder production[8].

The team led by Akash Yadav conducted research on the performance of a DC non-transferred thermal plasma torch. They constructed a two-dimensional steady-state axisymmetric model that encompassed gas injection, the internal region, and the environmental jet. The consistency between numerical simulation and experimental data verified the accuracy of the model, revealing the role of Lorentz forces in accelerating and constricting the jet. The study evaluated the impact of the cooling coefficient on jet temperature, efficiency, and operating conditions, determining the optimal cooling coefficient for balancing electrode life and thermal efficiency. A comparative analysis of the influence of different working gases on jet characteristics was conducted, concluding that argon plasma torches have advantages in terms of temperature and jet length [9].

The team led by S. Elaissi used CFD simulations to study the impact of working gases and operating conditions on the flow behavior of a DC plasma torch, aiming to optimize the design for enhanced stability. The results indicated that the type of carrier gas determines the arc length, and a stable arc requires low current, high voltage, low flow rate, and strong swirl. Reducing the inlet radius can increase the axial flow velocity, leading to the extension of the arc attachment point [10].

2. Core Parameters for Numerical Simulation of DC Arc Plasma Torch

2.1. Material

For plasma materials, different working gases correspond to different densities, specific heat capacities, viscosity coefficients, thermal conductivities, and electrical conductivities (their symbols are represented from left to right as follows: ρ , c_p , μ , κ and σ). Due to the experimental measurements of plasma properties for different gases by the Murphy A B professor's team, these properties are introduced into the numerical calculation software using a piecewise linear fitting method as required. It is particularly important to note that among these parameters, the electrical conductivity needs to be given a relatively small value at room temperature to ensure that the gas remains conductive even at room temperature.

2.2. Boundary Conditions

In the Fluent calculation, a mass flow inlet is used as the inlet boundary condition, and a pressure outlet is used as the outlet boundary condition. DC arc plasma torches can be mainly classified into two types: transfer arc and non-transfer arc. The main focus of this study is on the non-transfer arc, so the related parameters given are applicable to the non-transfer arc plasma torch. The inlet boundary can be set with velocity, pressure, and mass flow rate as the inlet conditions, while the outlet boundary can be set with a pressure outlet. Since many experimental researchers use flow meters to monitor inlet parameters, using a mass flow inlet is more consistent with reality.

The core components of a DC non-transfer arc plasma torch are the cathode, anode, intermediate electrode (inserted segment electrode), and insulator ring. Their structure is illustrated in Figure 1. In numerical calculations, it is necessary to set thermal boundary conditions for these components. The cathode wall needs to be set with heat flux and current density; the anode channel wall requires heat flux, and the temperature value for the anode outer wall can be obtained through experimental measurements. The intermediate electrode needs to determine the heat flux or wall temperature based on the heat transfer relationship with the external cooling medium; the insulator ring is treated as an adiabatic boundary, primarily because in the actual plasma torch, the insulator ring is made of a thermally conductive material such as plastic or ceramic, which is very poor in heat conduction, thus making the wall's thermal conductivity negligible.

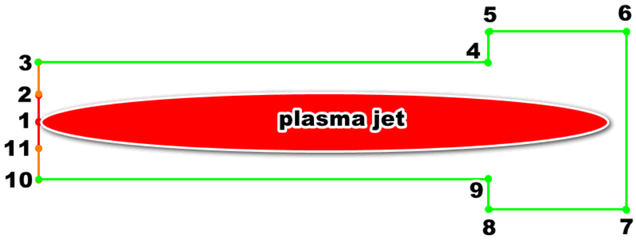

Figure 1. Schematic Diagram of a Two-Dimensional Planar Structure

Due to the numerous boundaries involved in the numerical calculation of the plasma jet, a table is used to record the specific values. The boundary parameter assignment table, as shown in Table 1, includes the following main entries: working gas 2-3; 10-11, jet exit 6-7, cathode front face 2-1-11, anode inner wall 3-4-5-6; 7-8-9-10.

Table 1. Boundary Parameter Assignment Table

Boundary	Temperature T/K	Velocity v	Potential φ	Pressure P/MPa
2-3; 10-11	300	m	γ	0.2-0.5
6-7	-	-	γ	0.1
2-1-11	3000	-	j_{cath}	-
3-4-5-6; 7-8-9-10	-	-	γ	-

Notes: m is the mass flow rate of the working gas, measured in kg/s. γ is flux representing Potential, $\gamma = {\partial\varphi}/{\partial n} = 0$.

2.3. Model Selection

Currently, in the industrial field, there are two types of plasmas commonly used: laminar plasma and turbulent plasma. Due to their different flow patterns, high-temperature regions, and jet velocities, they are used in different applications. For the first type, the laminar plasma, the appropriate flow model for computation is the laminar flow model. For the second type, the turbulent plasma, the influence of the viscous shear force at the wall must be considered, and the SST-k-w model is recommended. When studying the heat transfer and flow of a single jet, the simple solver can be used. When both the fluid domain of the jet and the solid domains of the cathode and anode are present, the coupled solver can be used for solution.

2.4. Common Basic Assumptions

For the numerical calculation of the internal flow field and temperature field of the plasma torch, the following assumptions and simplifications are made for the plasma's physical properties:

1) The arc plasma is assumed to be a continuum in local thermal equilibrium, and the flow and heat transfer are described by the N-S equations.

2) For laminar conditions of the arc plasma, a laminar flow model is employed. In turbulent conditions, standard k-ε, RNG k-ε, or SST k-w models can be used for computation, and the flow state can be either steady or unsteady.

3) All physical properties of the plasma are fitted with piecewise functions that depend on temperature.

4) Net radiation coefficients are used to calculate radiation heat losses, and the absorption of radiation by the arc is ignored.

5) Gravity terms, viscous dissipation, and pressure work are neglected.

6) Axial inlet is used inside the torch, which can be either non-swirling axial inlet or swirling inlet.

7) The plasma is treated as optically thin.

8) The effect of inductive electric fields is ignored.

3. DC Arc Control Equations

3.1. Mass Conservation Equation

$$\frac{\partial \rho}{\partial t} + \frac{\partial}{\partial x}(\rho v_x) + \frac{\partial}{\partial y}(\rho v_y) + \frac{\partial}{\partial z}(\rho v_z) = 0 \quad \text{(3-1)}$$

Equation (3-1) represents the mass continuity equation in a three-dimensional Cartesian coordinate system under unsteady flow conditions, where the first term is a non-zero term. If the first term is 0, then the equation represents the mass continuity equation under steady flow conditions. In the equation, ρ is the density, with units of kg/m³; v is the fluid velocity, with its components in the x, y, and z directions represented by v_x, v_y and v_z, respectively, with units of m/s.

3.2. The momentum conservation equation

The momentum equation in the x-direction is as follows:

$$\begin{aligned} &\rho \frac{\partial v_x}{\partial t} + v_x \frac{\partial}{\partial x}(\rho v_x) + v_y \frac{\partial}{\partial y}(\rho v_x) + v_z \frac{\partial}{\partial z}(\rho v_x) \\ &= -\frac{\partial P}{\partial x} + \frac{\partial}{\partial x}\left(2\mu \frac{\partial v_x}{\partial x}\right) + \frac{\partial}{\partial y}\left[\mu\left(\frac{\partial v_x}{\partial y} + \frac{\partial v_y}{\partial x}\right)\right] + \quad \text{(3-2)} \\ &\frac{\partial}{\partial z}\left[\mu\left(\frac{\partial v_x}{\partial z} + \frac{\partial v_z}{\partial x}\right)\right] + j_y \cdot B_z - j_z \cdot B_y \end{aligned}$$

The momentum equation in the y-direction is as follows:

$$
\begin{aligned}
&\rho\frac{\partial v_y}{\partial t}+v_x\frac{\partial}{\partial x}(\rho v_y)+v_y\frac{\partial}{\partial y}(\rho v_y)+v_z\frac{\partial}{\partial z}(\rho v_y)\\
&=-\frac{\partial P}{\partial y}+\frac{\partial}{\partial x}\left[\mu\left(\frac{\partial v_x}{\partial y}+\frac{\partial v_y}{\partial x}\right)\right]+\frac{\partial}{\partial y}\left(2\mu\frac{\partial v_y}{\partial y}\right)+\\
&\frac{\partial}{\partial z}\left[\mu\left(\frac{\partial v_y}{\partial z}+\frac{\partial v_z}{\partial y}\right)\right]+j_z\cdot B_x-j_x\cdot B_z
\end{aligned}
\tag{3-3}
$$

The momentum equation in the z-direction is as follows:

$$
\begin{aligned}
&\rho\frac{\partial v_z}{\partial t}+v_x\frac{\partial}{\partial x}(\rho v_z)+v_y\frac{\partial}{\partial y}(\rho v_z)+v_z\frac{\partial}{\partial z}(\rho v_z)\\
&=-\frac{\partial P}{\partial z}+\frac{\partial}{\partial x}\left[\mu\left(\frac{\partial v_z}{\partial x}+\frac{\partial v_x}{\partial z}\right)\right]+\frac{\partial}{\partial y}\left[\mu\left(\frac{\partial v_z}{\partial y}+\frac{\partial v_y}{\partial z}\right)\right]\\
&+\frac{\partial}{\partial z}\left(2\mu\frac{\partial v_z}{\partial z}\right)+j_x\cdot B_y-j_y\cdot B_x
\end{aligned}
\tag{3-4}
$$

In the equation, $j_y\cdot B_z-j_z\cdot B_y\,;j_z\cdot B_x-j_x\cdot B_z$ and $j_x\cdot B_y-j_y\cdot B_x$ which are the components of the Lorentz force $\vec{F}$ in the x, y, and z directions, respectively. That is $\vec{F}=\vec{j}\times\vec{B}$, where $\vec{B}$ is the magnetic flux density vector, with its components in the x, y, and z directions represented by B_x, B_y and B_z respectively.

3.3. The energy conservation equation

$$
\begin{aligned}
&\rho c_p\frac{\partial T}{\partial t}+\rho c_p\left(v_x\frac{\partial T}{\partial x}+v_y\frac{\partial T}{\partial y}+v_z\frac{\partial T}{\partial z}\right)\\
&=k\left(\frac{\partial^2 T}{\partial^2 x}+\frac{\partial^2 T}{\partial^2 y}+\frac{\partial^2 T}{\partial^2 z}\right)+\frac{{j_x}^2+{j_y}^2+{j_z}^2}{\sigma}\\
&+\frac{5k_B}{2e}\left(j_x\frac{\partial T}{\partial x}+j_y\frac{\partial T}{\partial y}+j_z\frac{\partial T}{\partial z}\right)+S_R
\end{aligned}
\tag{3-5}
$$

3.4. Turbulence model.

In the flow process, the SST k-ω turbulence calculation model within the Fluent software is used. The advantage of adopting this model is that it overcomes the shortcomings of the k-ε and BSL models, providing more accurate simulation predictions on the boundary layer. For plasma jets with a plateau stage, separation vortices may occur downstream of the plateau stage, and the SST k-ω model can accurately predict the initiation and magnitude of flow separation under adverse pressure gradients, thus playing a significant role in predicting jet flow separation. The transport equations for turbulent kinetic energy k and turbulent dissipation rate ω in the BSL k-ω model are as follows:

The transport equation for turbulent kinetic energy k is as follows:

$$
\frac{\partial}{\partial x_i}(\rho k u_i)=\frac{\partial}{\partial x_j}\left[\Gamma_k\frac{\partial k}{\partial x_j}\right]+G_k-Y_k
\tag{3-6}
$$

The transport equation for turbulent dissipation rate ω is as follows:

$$
\frac{\partial}{\partial x_i}(\rho\omega u_i)=\frac{\partial}{\partial x_j}\left[\Gamma_\omega\frac{\partial\omega}{\partial x_j}\right]+G_\omega-Y_\omega+D_\omega
\tag{3-7}
$$

In the equation Γ_k and Γ_ω represent the effective diffusivity, and its formulas are as follows:

$$
\Gamma_k=\mu+\frac{\mu_t}{\sigma_k}
\tag{3-8}
$$

$$
\Gamma_\omega=\mu+\frac{\mu_t}{\sigma_\omega}
\tag{3-9}
$$

$$
\mu_t=\alpha^*\frac{\rho k}{\omega}
\tag{3-10}
$$

Where D_ω is cross-diffusion term, the introduction of the cross-diffusion term is because of the blending of the standard k-ε model with the standard k-ω model. The specific formula for the cross-diffusion term is as follows:

$$
D_\omega=2(1-F_1)\rho\frac{1}{\omega\sigma_{\omega,2}}\frac{\partial k}{\partial x_j}\frac{\partial\omega}{\partial x_j}
\tag{3-11}
$$

Where the specific formula for the blending function F_1 is as follows:

$$
F_1=\tanh\left(\Phi_1^4\right)
\tag{3-12}
$$

$$
\Phi_1=\min\left[\max\left(\frac{\sqrt{k}}{0.09\omega y},\frac{500\mu}{\rho y^2\omega}\right),\frac{4\rho k}{\sigma_{\omega,2}D_\omega^+y^2}\right]
\tag{3-13}
$$

The SST k-ω includes all the improvements of the BSL k-ω, and the BSL k-ω encompasses both the standard k-ε and standard k-ω models. On this basis, the BSL k-ω considers the transfer of turbulent shear stress in the definition of turbulent viscosity. Compared to the aforementioned turbulence models, the SST k-ω turbulence model is more accurate and reliable, applicable to a wider range of flow regimes. The formula for creating turbulent viscosity is as follows:

$$
\mu_t=\frac{\rho k}{\omega}\frac{1}{\max\left[\frac{1}{\alpha^*},\frac{SF_2}{a_1\omega}\right]}
\tag{3-14}
$$

$$
F_2=\tanh\left(\Phi_2^2\right)
\tag{3-15}
$$

$$
\Phi_2=\max\left[2\frac{\sqrt{k}}{0.09\omega y},\frac{500\mu}{\rho y^2\omega}\right]
\tag{3-16}
$$

3.5. Electromagnetic equations

Under steady flow conditions, the current continuity equation is:

$$
\frac{\partial}{\partial x}\left(\sigma\frac{\partial\varphi}{\partial x}\right)+\frac{\partial}{\partial y}\left(\sigma\frac{\partial\varphi}{\partial y}\right)+\frac{\partial}{\partial z}\left(\sigma\frac{\partial\varphi}{\partial z}\right)=0
\tag{3-17}
$$

The Maxwell's equations are:

$$\begin{cases} 0=\dfrac{\partial}{\partial x}\left(\dfrac{\partial A_x}{\partial x}\right)+\dfrac{\partial}{\partial y}\left(\dfrac{\partial A_x}{\partial y}\right)+\dfrac{\partial}{\partial z}\left(\dfrac{\partial A_x}{\partial z}\right)+\mu_0 j_x \\ 0=\dfrac{\partial}{\partial x}\left(\dfrac{\partial A_y}{\partial x}\right)+\dfrac{\partial}{\partial y}\left(\dfrac{\partial A_y}{\partial y}\right)+\dfrac{\partial}{\partial z}\left(\dfrac{\partial A_y}{\partial z}\right)+\mu_0 j_y \\ 0=\dfrac{\partial}{\partial x}\left(\dfrac{\partial A_z}{\partial x}\right)+\dfrac{\partial}{\partial y}\left(\dfrac{\partial A_z}{\partial y}\right)+\dfrac{\partial}{\partial z}\left(\dfrac{\partial A_z}{\partial z}\right)+\mu_0 j_z \end{cases} \quad (3\text{-}18)$$

In equation (3-18), the current density can be obtained from Ohm's law, and the specific expression is as follows:

$$\begin{cases} j_x=-\sigma\dfrac{\partial\varphi}{\partial x} \\ j_y=-\sigma\dfrac{\partial\varphi}{\partial y} \\ j_z=-\sigma\dfrac{\partial\varphi}{\partial z} \end{cases} \quad (3\text{-}19)$$

4. Summary

As the flow rate of the working gas increases, the temperature of the plasma jet also increases, but the increase in flow rate does not lead to a significant rise in the maximum temperature. At the same time, the total gas volume within the arc chamber rises. Since the channel diameter of the arc chamber remains unchanged, this results in an increase in the thickness of the cold gas layer around the arc. The thickening of the cold gas layer enhances the compressive effect on the arc, which in turn leads to a decrease in the arc diameter. Throughout this process, the operating current of the plasma torch remains constant.

Due to the decrease in arc diameter while the total current needs to remain constant, the current density at the axis of the plasma torch must necessarily increase. The increase in current density leads to an enhancement of the arc's joule heating effect. As the arc is the energy source of the high-temperature plasma, the enhancement of its heating effect directly results in an increase in the temperature of the high-temperature plasma. Therefore, it can be concluded that the increase in the temperature of the high-temperature plasma is caused by the increase in current density.

As the working current increases, the temperature of the plasma gradually rises, indicating that the magnitude of the working current has a significant impact on the temperature of the high-temperature plasma. As the working current continues to increase, it is observed that the rate of increase in the temperature of the high-temperature plasma begins to decrease. This phenomenon can be attributed to the fact that, in the initial stage of current increase, the plasma temperature rises rapidly, which leads to a significant enhancement of the radiative heat loss effect.

As the radiative heat loss effect intensifies, its constraining influence on the rise in high-temperature plasma temperature becomes increasingly apparent. Consequently, even though the working current continues to increase, the rise in high-temperature plasma temperature is curtailed due to the increase in radiative heat loss. This results in the rate of increase becoming progressively smaller. Ultimately, this limiting effect of radiative heat loss causes the rate of increase in high-temperature plasma temperature to gradually level off.

During the operation of the plasma torch, if the flow rate of the working gas remains constant, there is no significant change in the thickness of the cold gas layer around the arc and the diameter of the arc. Therefore, when the arc current increases, due to the unchanged cross-sectional area of the arc channel, the current distribution becomes more dense, leading to a corresponding increase in the current density at the internal axis.

Many research scholars have used numerical simulation methods to study the influence of working gas flow rate, working current magnitude, degree of gas swirl, and non-swirling gas on the internal physical fields of the plasma torch. When all other operating condition parameters are the same, the temperature, current density, plasma flow velocity, and pressure within the plasma torch all increase with the increase of the working gas flow rate and working current. Under the same operating conditions, an increase in the degree of gas swirl will lead to a decrease in the internal temperature and current density of the plasma torch. Therefore, for the swirl inlet method, it is necessary to control the number of swirl channels and the inlet flow rate.

References

[1] Wang Zhen, Cao Wei, Li Yaojian. Numerical simulation study of the physical fields in a direct current arc plasma torch [J]. Industrial Heating, 2023,52(11):17-21. In Chinese.

[2] Shi Haoyang, Wang Pingyang, Wang Shu. Numerical Simulation and Diagnostics of Direct Current Arc Plasma Torch [J]. Shanghai Aerospace (Bilingual, Chinese and English) , 2024,41(01):122-129.DOI:10.19328/j.cnki.2096-8655.2024.01.016.

[3] K. B ,H. H ,R. S D .Numerical Investigation of the Effect of a Nozzle Extension on the Plasma Jet in Multi-Arc Plasma Spraying[J].Journal of Thermal Spray Technology, 2023, 32(6): 1856-1863.

[4] Manzke S, Krümmer M, Urlau F, et al. Numerical study of a plasma jet for plasma-assisted laser cutting[J]. Welding in the World, 2023, 67(7): 1667-1677.

[5] Zhang Z, Sun Q, Wang C, et al. Numerical Simulation and Experimental Study on a DC Multi-Cathode Arc Plasma Generator [J]. Plasma Chemistry and Plasma Processing, 2024, 44(1): 159-175.

[6] Wang X ,Ding J .Numerical simulation of magnetization induction coupled discharge plasma discharge process [J]. Applied Mathematics and Nonlinear Sciences, 2024,9(1):

[7] Xiao H, Ye Z, Xu C, et al. Numerical Simulation and Experimental Study of DC Arc Plasma Torch Thermal Efficiency[C]//Annual Conference of China Electrotechnical Society. Singapore: Springer Nature Singapore, 2022: 555-565.

[8] Abiyazhini R ,Sowmiya K ,Ramachandran K , et al.Numerical Comparison Between Characteristics of CO_2 and Ar Plasma Arcs With Anode Evaporation[J].IEEE Transactions on Plasma Science,2020,PP(99):1-9.

[9] Akash Y ,Sujay K , Satyananda K , et al. Numerical modelling of a direct current non-transferred thermal plasma torch for optimal performance[J].Contributions to Plasma Physics, 2022, 63(1):

[10] S. E ,I. A ,H. A , et al. Magneto hydrodynamic Simulation of Plasma Torch Used for Waste Treatment[J].Plasma Physics Reports,2021,47(7):704-714.